Crystallization dynamics of MAPbI3 perovskite solar cells via solvent engineering methods

DOI: 10.46932/sfjdv5n11-024

Received on: Oct 4th, 2024
Accepted on: Oct 25th, 2024

Stellah Wanyonyi
Bachelor of Education Science
Institution: Masinde Muliro University of Science and Technology
Address: Kakamega, Kenya
E-mail: stellahwanyonyim@gmail.com

Benard Omogo
PhD in Chemistry
Institution: University of Arkansas
Address: Fayetteville, Arkansas, United States
E-mail: bomogo@mmust.ac.ke

Celline Awino
Doctor of Natural Science (Renewable Energy)
Institution: Technical University of Berlin
Address: Berlin, Germany
E-mail: cawino@mmust.ac.ke

Miller Shatsala
Master of Science in Physics
Institution: Masinde Muliro University of Science and Technology
Address: Kakamega, Kenya
E-mail: millershatsala@gmail.com

Milimo Amos Nalianya
Master of Science in Physics
Institution: Masinde Muliro University of Science and Technology
Address: Kakamega, Kenya
E-mail: amuoso@gmail.com

Fred Ayodi Lisouza
PhD in Analytical Chemistry
Institution: Maseno University
Address: Maseno, Kenya
E-mail: flisouza@mmust.ac.ke

Abok Silas Odhiambo
Bachelor of Science in Physics
Institution: Masinde Muliro University of Science and Technology
Address: Kakamega, Kenya
E-mail: aboksilas1996@gmail.com

Francis Magiri Gaitho
PhD in Computational Physics
Institution: School of Chemistry and Physics, University of KwaZulu Natal (UKZN)
Address: Scottsville, South Africa
E-mail: fgaitho@mmust.ac.ke

ABSTRACT
Perovskite materials have attracted interest in solar cells due to ease of processing from salts. However, the complex crystal formation of perovskite from solvents is poorly understood. Solvent engineering approach to determine the crystallization dynamics and orientation of $MAPbI_3$ films using grazing incidence wide angle x-ray scattering (GIWAXS) and micro diffraction measurements were studied. The study further probes the effect of moisture, PTAA and PEDOTS: PSS hole transport layers on the stability of $MAPbI_3$ films. Precursor solutions were prepared by dissolving MAI and PbI_2 in pure DMF and mixture of DMF: DMSO in 4:1 v/v. Chlorobenzene and Ethyl acetate were used as antisolvent. Films prepared from DMF: DMSO mixture showed no PbI_2 signature while those prepared from DMF only, showed PbI_2 signature at q= 0.9 A^{-1}. This was attributed to solvent engineering of DMF/DMSO that leads to the formation of MAI/PbI_2/DMSO intermediate that delays the crystallization and promotes vertical growth of films. q= 0.9 A^{-1} signal was associated with high volatility of DMF which led to faster but discrepant nucleation and crystallization rate. Microdiffraction results showed insignificant influence of antisolvent on the perovskite structure. Humidity has a strong influence on the stability of $MAPbI_3$ films. PbI_2 intensity in the GIWAXS maps increased with increasing humidity while $MAPbI_3$ intensity decreased. This implied increased degradation of $MAPbI_3$ film with humidity due to recombination of charge carriers. A band gap of 1.57 eV, efficiency of 8.5% and E_t of 26 meV were obtained. Films with good crystallization are desirable in solar cells.

Keywords: $MAPbI_3$, Perovskite, Solvent Engineering, Crystallinity.

1 INTRODUCTION

Solvents are used to dissolve salts to form precursor solutions of perovskite. The main function of solvent is to dissolve the reagents and to participate in the perovskite crystallization process Different solvents have different rates of evaporation which highly influence the crystallization process.

The role of the solvent is not only to dissolve the reagents but also to participate in the perovskite crystallization process. Commonly used solvents in perovskite formation process are N, N- dimethyl formamide (DMF), dimethyl sulfoxide (DMSO) and Gamma butyrolactone (GBL). The complex interactions between solvents give insights in understanding their effects on the reproducibility and optimization conditions during perovskite fabrication. DMF solvent leads to random orientation of perovskite grains in the inner layer of perovskite films. This is caused by the fast volatilization of DMF (Liu; Xu, 2020). However, by the binary solvent engineering of DMF/DMSO, the formation of intermediate MAI/PbI_2/DMSO can delay the crystallization process to impel the vertical growth of subsequent crystallization in the inner layer of perovskite films (Lee *et al*., 2016). This leads to highly oriented films with high efficiency. Polar aprotic solvents can act as Lewis bases binding to Pb^{2+} acting

in turn as the corresponding Lewis acid. DMF has an almost ten times higher vapour pressure compared to DMSO leading to a higher processing window of $MAPbI_3$ (Dunlap-shohl, 2019). In this work, N, N-dimethyl formamide (DMF) and dimethyl sulfoxide (DMSO) were used to dissolve perovskite.

Anti-solvent engineering is an effective means of boosting the PCE of solar cells (Konstantakou *et al*., 2017; Heo *et al*., 2015). Anti-solvents are employed in perovskite to facilitate the removal of the host solvent in the precursor solution which makes the solution supersaturated and form large and dense homogeneous films and initiate crystallization of the perovskite film. Anti solvent treatment increases the nucleus density during film formation to produce uniform and pinhole-free perovskite film, which facilitates improved solar cell efficiency, low hysteresis, and stability. The physical properties of anti-solvents play a key role in controlling film morphologies. Non-polar solvents do not dissolve perovskite precursors (PbI_2 and CH_3NH_3I). However, non-polar solvents are quite miscible with DMF hence removes the residual solvents of DMF readily increasing the nucleation of perovskite therefore promoting crystallization of the perovskite films (Heo *et al*., 2015). Chen *et al.* (2018) prepared a highly efficient and stable $MAPbI_3$ perovskite solar cell using Ethyl acetate (EA) as anti-solvent with DMSO solvent and observed the influence of EA on the formation of smooth and transparent film perovskite films. Similarly, Chen *et al.* (2018) & Heo *et al*. (2015) fabricated perovskite materials using EA antisolvent on $MAPbI_3$ film. EA led to controlled nucleation and crystal growth process hence enhancing the morphology of the films leading to a better PCE. However, EA is less polar hence does not dissolve precursors leading to presence of PbI_2 in the perovskite films.

Anti-solvent with high boiling points induces slow growth of crystals during spin coating thus inhibiting the generation of cracks which leads to large crystals formation in the thin films and reduces recombination of electrons and holes in the films.

Chlorobenzene (CB) with a high boiling point of 131 $^{\circ}$ C makes it a better anti-solvent compared to EA with a boiling point of 77 ^{o} C. However, the use of CB is limited due to its high toxicity. Wu et al. used chlorobenzene anti-solvent in one step spin coating by dripping at different times which resulted in the formation of microporous structures at the bottom of the perovskite layer which was very significant to the quality of the perovskite film obtained (Wu *et al*., 2021).

Singh *et al*. (2023) used synchrotron Grazing incidence wide angle x-ray scattering (GIWAXS) to study the crystallization dynamics of triple cation films formed from pure DMF and DMF: DMSO; 4:1 v/v ratio with and without antisolvent (Singh *et al*., 2023) With DMF, GIWAXS showed intermediate phases while no intermediate phases were observed from DMF: DMSO, 4:1 v/v.

This research seeks to address the influence of solvent and antisolvent on the structure and crystal formation of $MAPbI_3$ perovskite films. The study further probes the effect of humidity on the crystallization kinetics and phase segregation of $MAPbI_3$ using GIWAXS and micro-diffraction synchrotron techniques

through variation of anti-solvent treatments. The study also aims at studying the effect of PTAA and PEDOTS: PSS hole transport layers on the stability of $MAPbI_3$ films in ambient environment. This is to help alleviate phase instability issues inherent in $MAPbI_3$ based perovskite solar cells.

2 THEORETICAL FRAMEWORK

Solvent engineering has been employed several research to determine the crystallization dynamics of perovskite films and improve the efficiency of the perovskite cells. Rong *et al*. (2015), used a mixed solvent of DMSO/DMF in making the $MAPbI_3$ perovskite precursor solutions and achieved $MA2Pb_3I_8{\cdot}2DSMO$ intermediate phase, which provided a unique treatment solution during film formation. Liu *et al*. (2020) used chlorobenzene to improve the PSCs performance. This also increased the film thickness and grain size. Zhang *et al*. (2023) obtained efficient and stable $MAPbI_3$ perovskite solar cell by use of green antisolvent diethyl carbonate with PCE of 20.20% and efficiency of 86% on exposure to ambient conditions for over 20 days.

These studies focus on improving the stability and PCE of the perovskite solar cell. However, the complex crystal formation of perovskite from solvents is poorly understood. Therefore, this study aims at addressing the influence of solvent and antisolvent on the structure and crystal formation of $MAPbI_3$ perovskite films. The study further probes the effect of humidity on the crystallization kinetics and phase segregation of $MAPbI_3$

3 METHODS AND MATERIALS

Bare glass substrates coated with indium tin oxide (ITO) were subsequently cleaned in acetone, detergent of 2% mucosal, deionized water and isopropanol for 20 minutes each. After each cleaning step, the samples were dried under nitrogen and thereafter treated with ultraviolet (UV) ozone for 20 minutes.

$MAPbI_3$ perovskite films were prepared according to Jeon *et al*. (2014) Precursor solutions of $MAPbI_3$ were prepared by dissolving 1.0M Methylammonium iodide, CH_3NH_3I (MAI, Sigma Aldrich, 99.99% purity) and 1.0 M lead iodide, PbI_2 (99.99 %, TCI) in DMF (99.99 %, Sigma Aldrich) and in a mixture of N, N- dimethyl formamide (DMF) and dimethyl sulfoxide (DMSO, Sigma-Aldrich) in 4:1 volume ratio respectively. The precursor solutions were stirred at 60°C for 12 h in a nitrogen filled glove box. Before perovskite deposition, the temperature of glovebox atmosphere was kept at about 28 °C. 50 µl of the precursor solution was spin coated onto a 15 mm by 15 mm substrate at 4000 rpm for 25s. 10s to the end of spin coating process, 210 µl of chlorobenzene or Ethyl acetate were dripped to the substrate while spinning in the final stage. After that, $MAPbI_3$ films were formed during annealing at 100°C for 10

min (Kegelmann *et al*., 2017). PEDOTS: PSS (Poly(3,4-ethylenedioxythiophene) Polystyrene sulfonate) and PTAA (Poly(triarylamine) were used as hole transport layers (HTL). 30µl of the stock solution of PEDOTS: PSS (Clevious Al 4083, Heraus) was spin coated on the cleaned ITO substrate at 3000 rpm for 60 seconds and then heated on a hot plate at 135 °C for 20 minutes (Bi *et al*., 2014) and cooled to room temperature. PTAA was prepared by dissolving 15 mg into 1 ml of toluene. 3.4µl of 4-tert-butylpyridine (TBT), 13.6 µl Li-bis (trifluoro methane sulfonyl) imide, Li-TSFI) and 28.3 mg/ml acetronile were added and spin coated on the ITO substrate at 3000 rpm for 30 seconds. (Heo *et al*., 2013).

Scanning electron microscopy (SEM), Grazing incidence wide angle x-ray scattering (GIWAXS) and microdiffraction techniques were used for characterization. SEM pictures were measured using Bruker at 5kV acceleration voltage, and current of 10 µA with a magnification of 64.44 kx for top view measurements.

Grazing incidence wide angle x- ray scattering (GIWAXS) measurement was performed at the 7.3.3 beam line at the advanced light source (ALS) of the Lawrence Berkeley National laboratory (LBNL). The energy of the X-ray used was 10 keV with a current of 500 mA. The scattering signal was collected using a Dectris Pilatus 2M detector and integrated to reduce to 1D using NIKA GIWAXS software. The diffracted signal is in a punctual out of plane detector as a function of detector angle. For GIWAXS, the signal was collected by an area detector at a fixed position which gave additional information about the Crystal orientation. The moisture was controlled using a helium purge onto the chamber and the relative humidity monitored through a humidity sensor. GIWAXS analysis was done between an angle of 0.1° to 0.5 °to get sufficient information of the diffraction patterns at the bulk of perovskite sample hence probing the crystal orientation of the sample. The 2-D GIWAXS detector images was calibrated with silver behenate (AgB) and converted into the q-space and typical azimuthal averaging or line cuts to form a 1-D intensity versus q which allowed for more qualitative analysis of peak evolution during crystallization (Coffey, 2023). Igor Pro software was used for data analysis.

The synchrotron-based X-ray micro-diffraction experiment was conducted at the Beamline 12.3.2 at the Advanced Light Source (ALS), Berkeley Lab, CA. A 10 keV monochromatic X-ray beam was used to measure the structural behavior of perovskite material. The monochromator and Kirkpatrick-Baez (KB) mirrors were placed inside a compact Plexiglas box filled with a helium atmosphere to improve thermal stability and reduce X-ray air scattering and absorption. The diffraction patterns were collected with a Pilatus 1M detector. The sample was usually mounted in a 45°active geometry. The CCD was placed on a vertical slide at approximately 35 mm from the sample area illuminated by the beam. This allows for the collection of a large solid angle of the reciprocal space without having to move the detector.

Modulated SPV measurements were done by modulated SPV spectroscopy where illumination was performed with a halogen lamp (100 W) and quartz prism monochromator (SPM2) at a frequency of

8 Hz with a quartz cylinder reference electrodes partially coated with conductive SnO2: F (band gap about 3.6 eV). The reference electrodes related to the high-impedance buffer with a capacitance of the measurement capacitor between 10 and 20 pF. The signals were detected with a high frequency buffer (input resistance 50 GΩ) and a double phase lock-in amplifier (EG&G 5210) (Dittrich *et al*., 2015). SPV Spectra were measured in a wide range (0.4 – 4.0 eV, step 50 meV) and in a narrow range (around the band gap, step 10 meV). Widths of the entrance and exit slits of the monochromators were set to 0.3 mm (spectral resolution better than 10 meV).

4 RESULTS AND DISCUSSION

4.1 EFFECTS OF PRECURSOR SOLVENTS ON THE CRYSTALLIZATION ORIENTATION AND STRUCTURE OF $MAPBI_3$

Figure 1 shows the GIWAXS images (a and b) and Intensity versus q value (c and d) for $MAPbI_3$. From Figure 1 (a), the maps showed an extra peak between 1.0 and 0.5 with a high intensity (marked green star). This probably might be due to the presence of undissolved PbI_2. This is also supported by the presence of the (001) PbI_2 peak as observed in the GIWAXS spectrum peaks shown in the Figure 1 (c). A peak at Q vector (A^{-1}) equals to 0.9 indicates the presence of PbI_2 in the structure, while a peak at Q vector (A^{-1}) equals to 1.0 indicates the presence of $MAPbI_3$ perovskite film. The presence of the (001) PbI_2 could be associated with high volatility of DMF which led to fast but discrepant nucleation and crystallization rate thus leading to formation of PbI_2 in the film (Huang *et al*., 2021; Ahn *et al*., 2018). Secondly, the solubility of PbI_2 in DMF is low hence the presence of undissolved PbI_2 in the precursor solution.

On the other hand, no PbI_2 signature observed when MAI and PbI_2 were dissolved in a mixture of DMF-DMSO with high intensity of $MAPbI_3$ perovskite film formation (see Figure 1 (b) and (d)). This could probably be attributed to the binary solvent engineering of DMF/DMSO that leads to the formation of intermediate MAI/PbI_2/DMSO phase which delays the crystallization process to impel the vertical growth of subsequent crystallization in the inner layer of perovskite films (Huang *et al*., 2021). This leads to highly oriented films which are completely converted to $MAPbI_3$ with no PbI_2 phase hence high efficiency. Studies have also shown that mixing DMF with small amounts of DMSO results in the formation of high iodine-coordinated iodo-plumbates together with the corner sharing PbI_2 complexes which acts as nucleation sites for $MAPbI_3$ (Singh *et al*., 2023).

Figure 1: GIWAXS image of $MAPbI_3$ when (a) DMF used as a solvent (b) DMF-DMSO used as a mixed solvent (c) GIWAXS peaks obtained from $MAPbI_3$when DMF used as solvent alone and d) peaks obtained from $MAPbI_3$ when using mixed solvents of DMF-DMSO.

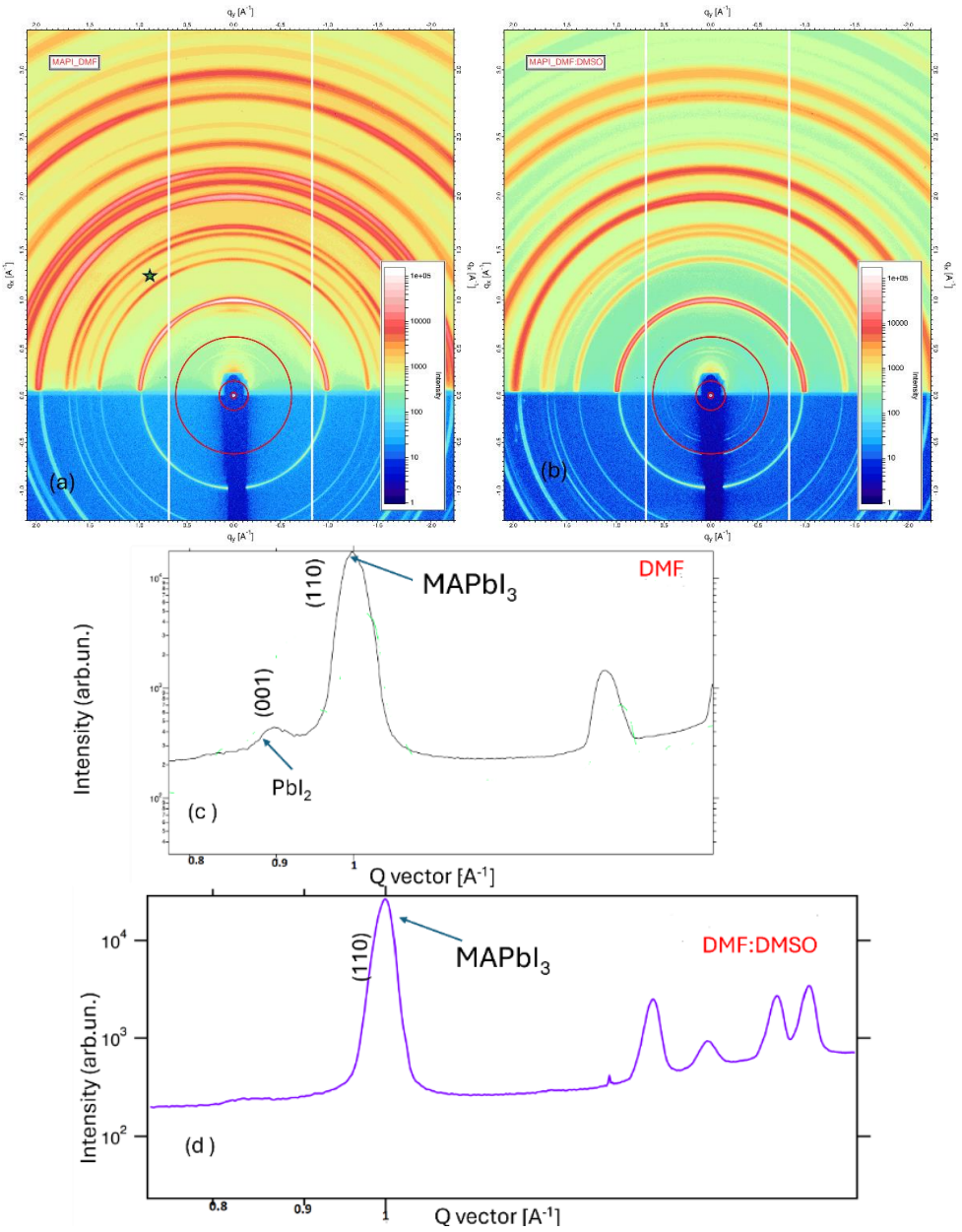

Source: The authors.

4.2 EFFECTS OF ANTI-SOLVENTS ON CRYSTALLINITY AND MORPHOLOGY OF $MAPBI_3$ FILM

Figure 2 (a) shows GIWAXS map of $MAPbI_3$ when EA was used as antisolvent. The perovskite ring at q vector equals 1.0 A^{-1} is of low intensity as compared to when CB was employed as antisolvent (see Figure 2 (b)). In Figure 2(b), there is the appearance of a bright and dominant ring of higher intensity at q vector equals to 1.0 A^{-1}. These results agree with the fact that EA is less polar, does not dissolve precursors leading to appearance of pbI_2 in the film and weak formation of perovskite films. This was

attributed to the low boiling point of EA which makes the crystallization process rapid but discrepant nucleation and crystallization rate (Wu *et al*., 2021). This also hinders grain growth of the perovskite film thus resulting in more cracks leading to increased recombination rate. This leads to poor morphological properties of $MAPbI_3$ film. Films produced by CB as an antisolvent produce a quality film with quality morphological properties.

Figure 2: GIWAXS Images of $MAPbI_3$ when DMF-DMSO used as solvent with (a) EA as an antisolvent and (b) CB as an antisolvent.

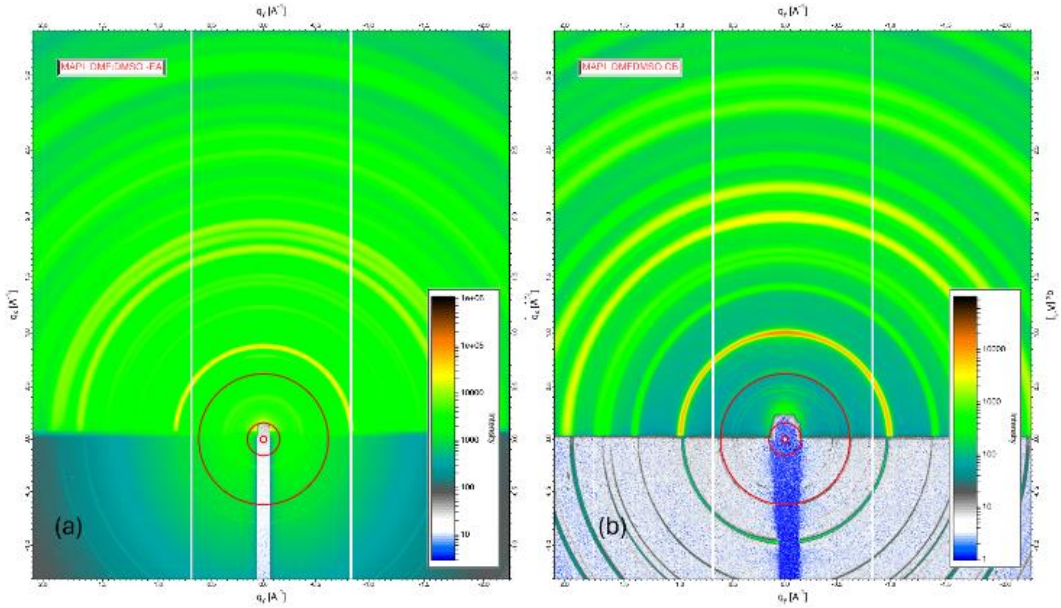

Source: The authors.

4.3 X-RAY MICRODIFFRACTION ANALYSIS

The microdiffraction analysis shown in Figure 3 depicts typical tetragonal peaks for $MAPbI_3$ dripped with antisolvent of chlorobenzene (CB) and ethyl acetate (EA). Several prominent peaks were observed at 14.2 °, 23.5°, 24.6°, 28.5°, 31.9°,35.1°, 40.7°, 43.4° and 50.4° corresponding to (110), (211), (202), (220), (310), (312), (224), (330) and (404) tetragonal peaks of $MAPbI_3$ perovskites, respectively. These peaks agree with the results reported by (Taylor *et al*., 2021; Fan *et al*., 2016). The peaks were similar for $MAPbI_3$ films with of anti-solvent of CB and EA. This implied that antisolvent had no significant influence on the micro-structure of perovskites.

It was also evident from the Xray microdiffraction spectrums that there was formation of $MAPbI_3$ crystalline structures in both CB and EA antisolvents due to formation of thin peaks. The intensity of the peaks was high considering the major peaks at (110), (220) and (310) indicating formation of large amounts of crystalline perovskite. This was also evident from the SEM images in Figure 4.

Figure 3: XRD spectrums for $MAPbI_3$ films with CB and EA antisolvents

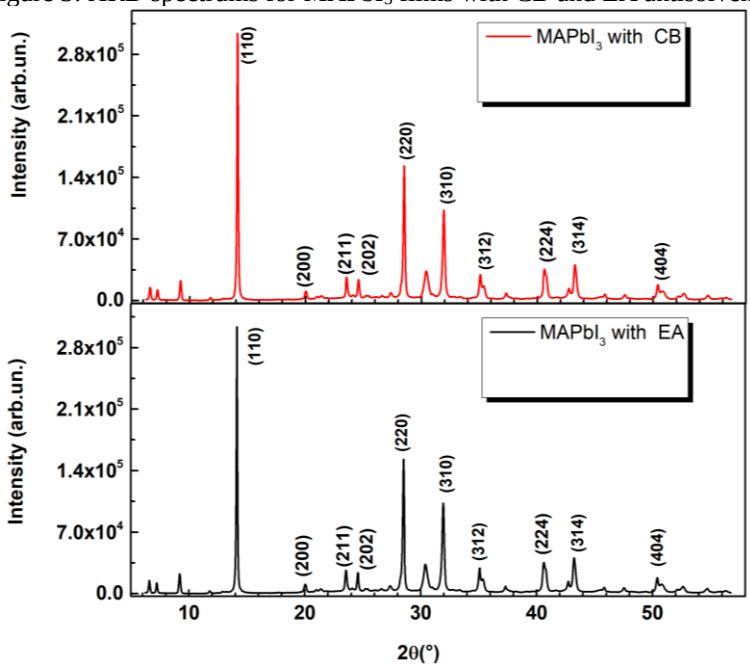

Source: The authors.

4.4 SCANNING ELECTRON MICROSCOPY (SEM)

It is a surface analytical technique used to study the morphology and composition of materials in modern science. Figure 4 shows images obtained from scanning electron microscopy for $MAPbI_3$ with CB and EA as antisolvent (see Figure 4 (a) and (b), respectively). The images in both figures showed the films were composed of large grains indicating high crystallinity, with desired film morphology and full surface coverage with less cracks hence less defects. These features significantly enhance light harvesting efficiency of the cell and reduce charge recombination. The largest grain measured about 500 nm. Larger grains are desirable for good performance in solar cells since the charge carriers will travel a larger distance before recombination takes place along the grain boundaries (Fan *et al*., 2016). When the grains are large, it means there is reduction in grain boundaries that acts as recombination sites for charge carriers hence larger diffusion length in the material. SEM images obtained show good adhesion of the $MAPbI_3$ film to the substrate and are relatively smooth with fewer pinholes. Smooth surface allows the film to absorb more light hence enhancing the light harvesting efficiency of cell (Omondi, 2018; Doumbia *et al*., 2022).

Figure 4: Scanning electron microscopy images for $MAPbI_3$ film with (a) CB and (b) EA.

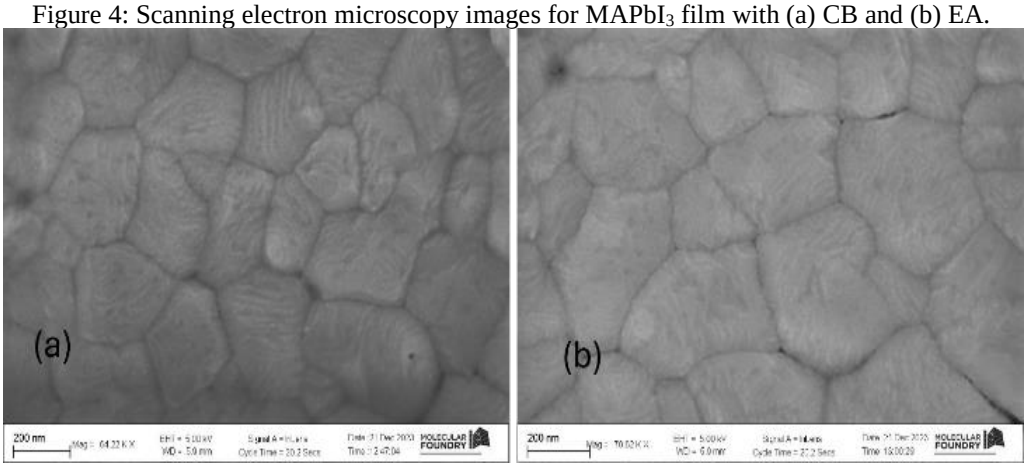

Source: The authors.

4.5 EFFECTS OF HUMIDITY ON DEGRADATION OF $MAPBI_3$ FILMS

Exposure of perovskite films to humidity accelerates the rate of degradation of the films. Humidity decomposes the $MAPbI_3$ film back to constituent MAI and PbI_2. To study the stability of the films, $MAPbI_3$ films were exposed to different humidity percentages and GIWAXS images were obtained as shown in Figure 5.

The maps in Figure 5 obtained from the GIWAXS measurements show without Relative Humidity (RH) $MAPbI_3$ does not show PbI_2 and intermediate phases as seen in (a) which is supported by the q-space plot in Figure 5. However, RH values of 13% (b), 45% (c), 89% (d), 104%(e) and 110% (d) for an exposure time of 10s, present distinct peaks at q (x,y) value of 1.0 A^{-1} which is a typical perovskite phase of (110) with slight peaks at q = $0.9A^{-1}$ corresponding to (001) phase as seen in Figure 5(b). It was also noted that, with increasing RH levels from 13% to 110%, $MAPbI_3$ perovskite phase (110) remains stable with slight shift back of (001) phase which is PbI_2 at 0.9 A^{-1}, and Figure 5(b) shows the PbI_2 peaks from the minimal phase shift of $MAPbI_3$. The intensity of PbI_2 in the GIWAXS maps increases with an increase in humidity percentage while the intensity of $MAPbI_3$ reduces as the percentage of humidity increases. This is due to the increased decomposition rate of $MAPbI_3$ perovskite film on exposure to humidity.

However, the peaks at 0.9 A^{-1} become clearer as the RH humidity is increased from 0% to 110% (see Figure 5 (a)), which demonstrates the (110) peak of $MAPbI_3$ with relatively low humidity tests, the result rightly rules out predator phases in the film, building confidence of non-segregation of the film back to the (001) phases. In Figure 5 (b-f), $MAPbI_3$ perovskite peak of (110) at q = 1.0 A^{-1} is still intensely seen with other smaller peaks appearing at q value of 0.9 A^{-1}. The small peak at q = $0.9A^{-1}$ was because of segregation of the films slightly back to the (001) phase which intensified as RH was increased to 51%. It was thus deduced that, although humidity influenced the crystallization of $MAPbI_3$, the crystals remain

slightly resistant to low value of RH stress and degrades to PbI_2 phase as RH values was increased up to 51%, with only (001) crystal planes appearing similar to other findings [17].

From Figure 6, it was observed that at 0% RH, there was dominant perovskite peak at q vector of $1A^{-1}$. However, when the film was subjected to relative humidity of 13%, 45%, 89% and 110%, the (110) $MAPbI_3$ peak at q vector of 1 A^{-1}, disappeared and there was appearance of (001) PbI_2 peak at q value of 0,9 A^{-1} and MAI peak at q value of 0.8 A^{-1}. The results agree with those reported by (Awino *et al*., 2017), suggesting that the perovskite films degraded to their constituent element (MAI and PbI_2) on application to relative humidity.

Figure 5: GIWAXS maps of $MAPbI_3$ when exposed to relative humidity (RH) of (a) 0% % (b) 13%; (c) 45% (d) 89% (e) 104% and (f) 110%

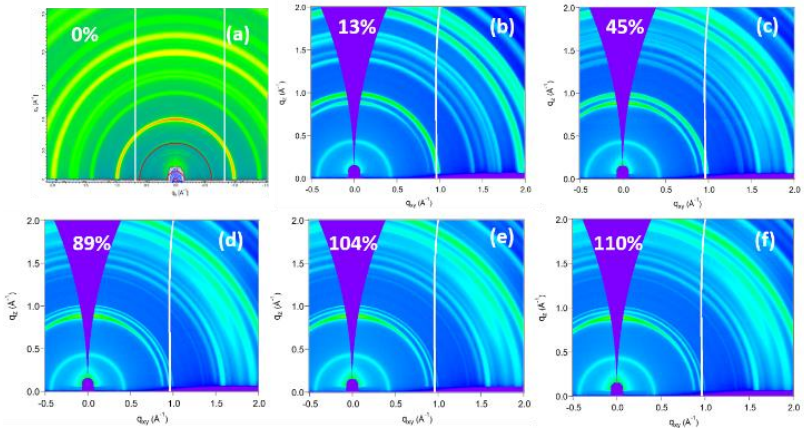

Source: The authors.

Figure 6: GIWAXS peaks of $MAPbI_3$ when exposed to different relative humidity (RH); (Blue line at 0 %, Magenta- 13%, light green- 45%, grey- 89% and red -110%)

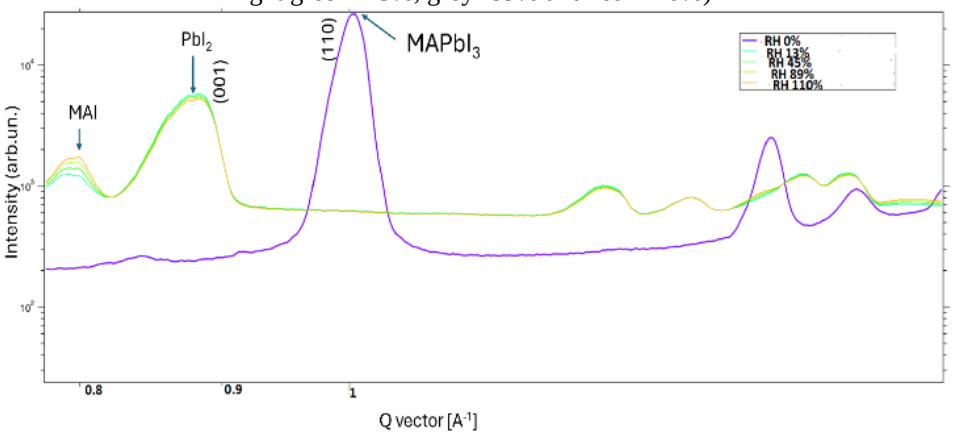

Source: The authors.

4.6 SURFACE PHOTOVOLTAGE SPECTROSCOPY

SPV spectra were obtained on $MAPbI_3$ with varying the HTL. The SPV spectra of PEDOT: $PSS/MAPbI_3/C_{60}/BCP_{evap}$ and $PTAA/MAPbI_3/C_{60}/BCP_{evap}$ (Figure 7 (a) and (b)). All the samples showed

an onset of the SPV signals at around 1.55eV which is close to the band gap of $MAPbI_3$ between 1.5 eV to 1.6eV (Shockley; Queisser, 2018). The in-phase signal (x-signal) of PEDOT: PSS/$MAPbI_3$/C_{60}/BCP_{evap} (Figure 7(a) was negative with a maximum magnitude of about 5.0mV at a photon energy of about 1.7 eV when freshly prepared. This indicates that photo-generated electrons were preferentially separated towards the external surface of the films with holes towards the substrate indicating a p-type semiconductor. The Shift by 90^o (Y signal) for the film has a positive value (opposite direction to the in-phase) implying that one mechanism of charge separation (Dittrich et al.,2015 & Awino et al., 2020). The Shift by 90^o (Y signal) has a smaller magnitude than in-phase signals suggesting that trapping and de-trapping of charge carriers may lead to slow response of the SPV spectra (Dittrich *et al*., 2015). On exposure to air for two days, the magnitude of the in-phase signal reduced to 3.8 mV. The reduction in phase signal magnitude of PEDOT: PSS/$MAPbI_3$ after two days in air is likely to be an indication of wider distribution of gap states of different types throughout the band gap. This may be caused by a long exposure time which degrades the PEDOT: PSS (Blazinic *et al*., 2019). Photo-oxidation of PEDOT: PSS leads to formation of sulfon group (SO_2) resulting in disruption of Л-conjugation in PEDOT: PSS and this leads to reduction in electrical conductivity (Marciniak *et al*., 2004). Figure7(b) showed PTAA/$MAPbI_3$/C_{60}/BCP_{evap} deposition with a negative in-phase signal at a maximum magnitude of about 2.3 mV, photon energy of about 1.7 eV when freshly prepared. High SPV signal obtained by PEDOT/$MAPbI_3$ deposition might be due to reduced transport energy barriers in PEDOTS: PSS and low density of photo-generated carriers in PTAA. PEDOTS: PSS has high electrical conductivity thus causing unwanted non-radiative recombination thus reduced recombination (Stranks *et al*., 2017). The signals for PTAA/$MAPbI_3$ increased on exposure to air after two days. This might be due to passivation of surface defects on continued to exposure to air (Awino *et al*., 2017).

Figure 7: SPV overview spectrum for (a) PEDOT: PSS/ $MAPbI_3$/C_{60}/BCPevap and (b) PTAA: $MAPbI_3$/C_{60}/BCPevap

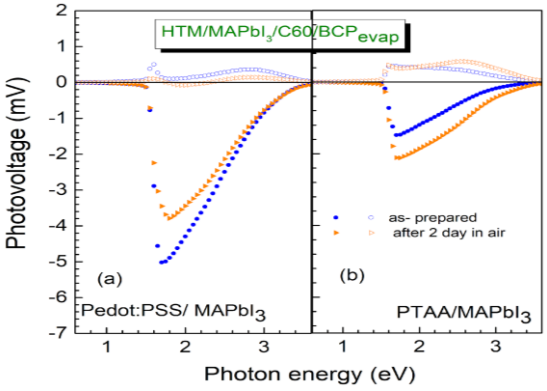

Source: The authors.

To determine the defect states below the band gap energy of the films, a plot of PV amplitudes divided by photon flux on a logarithmic scale as a function of photon energy for the in-phase signal of the

same samples were made (Figure 8). From the SPV spectra in Figure 8, the values of the band gap were about 1.57 eV for both $MAPbI_3$ deposited on PEDOT: PSS and PTAA as HTL which is close to the band gap of $CH_3NH_3PbI_3$ (Liu *et al*., 2017). The band gap remained the same even after exposure to air for two days. This indicates that the atmospheric environment had no effect on the band gap of the films. According to Figure 8 (b), an onset energy (E_{on}) of 1.45eV slightly below the band gap of the bulk.

Figure 8: The dependence of PV amplitude divided by photon flux as a function of photon energy for (PEDOT: PSS/$MAPbI_3$/C_{60}/BCP $_{evap}$ and (b) PTAA / $MAPbI_3$/C_{60}/BCP_{evap}

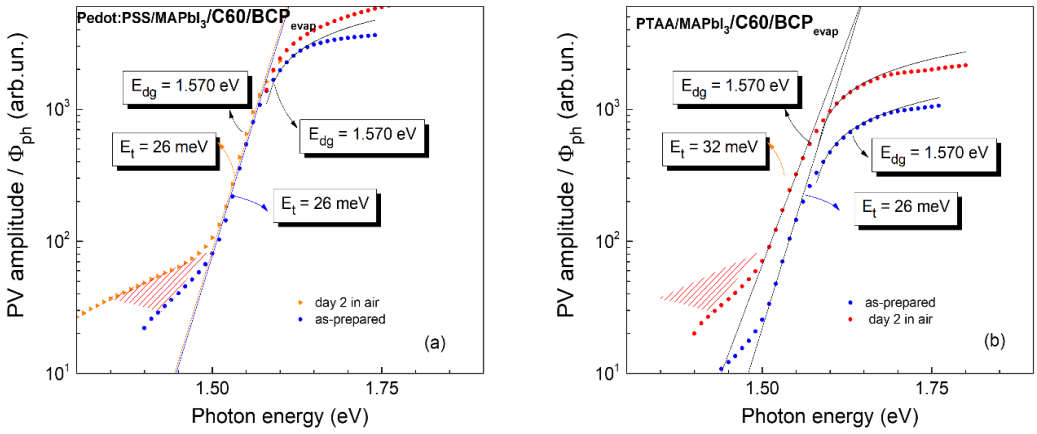

Source: The authors.

The onset energy (E_{on}) of PEDOT: PSS/ $MAPbI_3$ showed a very slight decrease therefore having no effect on the band tail (E_t) of the samples. A low band tail (E_t) of 26 meV was obtained for both samples of PEDOT: PSS/ $MAPbI_3$ and PTAA/ $MAPbI_3$ when prepared. This is comparable to the tail of states obtained by Awino *et al*. (2017) for Mo/$MAPbI_3$ /80mg/ml PMMA. This value is slightly higher than Urbach tail energy of 15 meV obtained by De Wolf *et al*. (2014). This indicates a higher degree of disorder obtained in our samples. Storage of the samples in air for two days had no effect on the tail of states for PEDOTS: PSS/$MAPbI_3$. The onset energy (E_{on}) for PTAA/$MAPbI_3$ reduced from 1.48 eV when prepared to 1.44 eV after storage in air for two days. This therefore increased the tail of states with storage in air for two days to 32 meV. Exposure of the film to air caused a strong increase of disorder due to $MAPbI_3$ stress which can be attributed to intrusion of moisture related impurities into the sample (Awino et al., 2017) caused by hygroscopicity of PTAA verses the large surface -tension and incomplete surface coverage of the photoactive perovskite film. This reduces the performance of the samples (Xu *et al*., 2022). Alternative explanation could be due to degradation at the perovskite/PTAA interface when HI gas is released from MAI (Wang et al., 2022)

Figure 9 showed the variability of band gap (Eg) for PEDOT: PSS/$MAPbI_3$/C_{60}/BCP $_{evap}$ and (b) PTAA / $MAPbI_3$/C_{60}/BCP_{evap} for different batches which were studied. $CH_3NH_3PbI_3$ deposited on PTAA displayed wider spread in Egas compared to $CH_3NH_3PbI_3$deposited on PEDOT: PSS.

Figure 9: The spread in band gap energy (Eg) in eV against for (PEDOT: PSS/$MAPbI_3$/C_{60}/BCP_{evap} and PTAA / $MAPbI_3$/C_{60}/BCP_{evap}

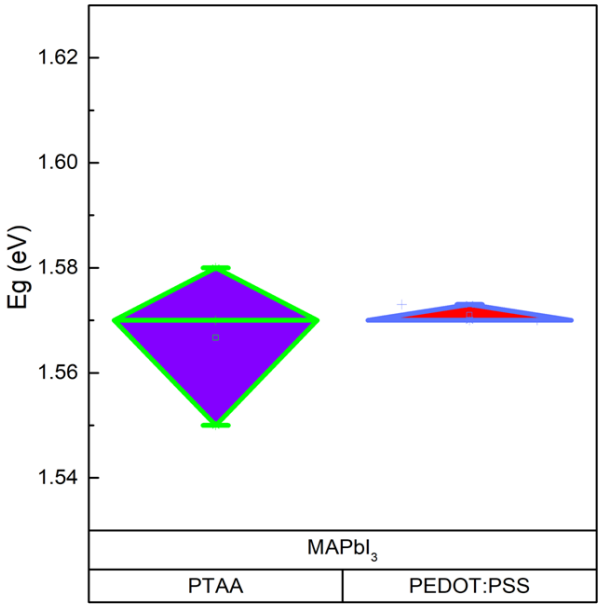

Source: The authors.

5 CONCLUSION

We have employed solvent engineering approach to control the crystallization process of perovskite films. Smooth, dense, homogeneous and highly crystalline films with good surface coverage were obtained with Mixed DMF: DMSO in 4:1 v/v ratio and chlorobenzene as antisolvent. Perovskite films with high level of phase purity and good crystallization is desirable in solar cells. The microdiffraction XRD pattern showed typical perovskite peaks at 14.2 °, 23.5°, 24.6°, 28.5°, 31.9°,35.1°, 40.7°, 43.4° and 50.4° corresponding tetragonal peaks of $MAPbI_3$ perovskites comparable to what was reported elsewhere (Awino *et al*., 2017). This Implied that $MAPbI_3$ films formed were highly crystalline with enhance microstructural properties desirable for making photovoltaic devices. Moreover, we also observed diffraction peaks at low angles in both CB and EA. This compared well with the result obtained by Ahn *et al*. (2015). We further observed that humidity has a significant effect on the stability of $MAPbI_3$ films. The intensity of PbI_2 in the GIWAXS maps increased with an increase in humidity percentage while the intensity of $MAPbI_3$ decreased as the percentage of humidity increases. This showed that there was increased degradation of $MAPbI_3$ perovskite film when exposure to humidity due to recombination of charge carriers reducing performance of $MAPbI_3$photovoltaic based devices. However, at low humidity, the films obtained were stable.

SEM micrographs showed homogeneous films with good surface coverage and large grains for both $MAPbI_3$ dripped with CB and EA as antisolvent. Films with larger grains further confirm high crystallinity of our films favorable in solar device applications.

In addition to the implications in solar cell performance, our result provides important insights in understanding the process of crystallization, nucleation and growth in $MAPbI_3$ films using Synchrotron based measurements. Solvents affect the nucleation and growth of perovskite films which in turn influences the size, purity, morphology and crystal structure. This makes it possible to develop reproducible perovskite solar cells with optimized physical, morphological and structural properties. Our study did not optimize film formation parameters including using broad range of precursor solvents, monitoring antisolvent dripping time and amount of antisolvent to be administered. We thus propose optimization of these parameters and to extend the study to 2D-3D perovskite for enhanced stability.

Recent DFT study showed that mixing DMF with small amounts of DMSO results in a better balance in the energies and more equilibria in the crystallization process forming good quality perovskite films(Ahn *et al*., 2015). This is confirmed by our results on GIWAXS maps and spectrum which showed high intensity of $MAPbI_3$ peaks with no signature of PbI_2. A possible explanation is that by mixing DMSO into the DMF, the coordination of DMSO with PbI_2 dominates and prevent the formation of intermediate phase and this serve as nucleation sites to form perovskite (Jiang *et al*., 2022). On the other hand, our result on GIWAXS maps and spectrum of pure DMF showed the appearance of PbI_2 due to weaker coordination of DMF with PbI_2 (Arain *et al*., 2019). Our results compare well with those reported by Singh *et al*. (2023).

Good quality films are critical for obtaining highly performing perovskite devices with good photovoltaic properties. Several studies have developed high quality crystalline thin film perovskites; however, they have not explicitly addressed structural degradation as observed in GIWAXS diffraction peaks caused by moisture because of hydrophilic nature of $MAPbI_3$ based perovskite. In this study, we have shown that humidity has a significant influence on the stability of $MAPbI_3$ films and can affect the photovoltaic performance of $MAPbI_3$ -based devices. Humidity can cause degradation of $MAPbI_3$ film to PbI_2 (Li *et al*., 2016; Toloueinia *et al*., 2020) as observed in the GIWAXS measurement where intensity of PbI_2 increased with humidity and result in the decline in device performance. Therefore, good knowledge of dissolving mechanism, length of antisolvent administration, environmental degradation pathways is vital in understanding the perovskite films formation to develop a stable, uniform, homogeneous and highly crystalline $MAPbI_3$perovskite solar cells.

SPV results showed high E_t of 32 meV in the structure of ITO/PTAA/$MAPbI_3$/C_{60}/BCP compared to 26 meV in the structure of ITO/PEDOT: PSS/$MAPbI_3$/C_{60}/BCP when exposed to air for two days. This was suggested to probably due to degradation at PTAA/ perovskite interface when hydrogen iodine (HI) is released from MAI. We thus recommend that MAI free perovskite may be used in future work.

ACKNOWLEDGEMENTS

We express our appreciation to the World Academy of Sciences (TWAS) research grant program (grant number 20-287 RG/PHYS/AF/AC-G-FR3240314167) for the financial support and availing the glove box which was a crucial equipment in this study.

Further appreciation goes to the to the Beamline 7.3.3 and 12.3.2 of the Advanced Light Source which is supported by the Director of the Office of Science, Office of Basic Energy Sciences, of the U.S. Department of Energy under Contract No. DE-AC02-05CH11231. Moreover, we sincerely thank the Molecular Foundry division, which is also supported by the Office of Science, Office of Basic Energy Sciences, of the U.S. Department of Energy under Contract No. DE-AC02-05CH11231 and Lawrence Berkeley national lab for providing equipment.

Celline Awino and Miller Shatsala express their appreciation to LAAAMP for the generous grant which played an important role in supporting this research project.

REFERENCES

Ahn, N., Jeon, I., Yoon, J., Kauppinen, E. I., Matsuo, Y., Maruyama, S., & Choi, M. (2018). Carbon-sandwiched perovskite solar cell. *Journal of materials Chemistry A*, *6*(4), 1382-1389.

Ahn, N., Son, D. Y., Jang, I. H., Kang, S. M., Choi, M., & Park, N. G. (2015). Highly reproducible perovskite solar cells with average efficiency of 18.3% and best efficiency of 19.7% fabricated via Lewis base adduct of lead (II) iodide. *Journal of the American Chemical Society*, *137*(27), 8696-8699.

Arain, Z., Liu, C., Yang, Y., Mateen, M., Ren, Y., Ding, Y., ... & Dai, S. (2019). Elucidating the dynamics of solvent engineering for perovskite solar cells. *Sci. China Mater*, *62*(2), 161-172.

Awino, C., Barasa, G., & Odari, V. (2020). Light induced degradation of the transport length of CH3NH3PbI3 studied by modulated surface photovoltage spectroscopy after Goodman. *Organic Electronics*, *77*, 105503.

Awino, C., Odari, V., Dittrich, T., Pongthep, P., Thomas, S., & Bernd, R. (2017). Investigation of structural and electronic properties of CH3NH3PbI3 stabilized by varying concentrations of poly (Methyl Methacrylate)(PMMA). *Coatings*, *7*(8), 115.

Bi, C., Shao, Y., Yuan, Y., Xiao, Z., Wang, C., Gao, Y., & Huang, J. (2014). Understanding the formation and evolution of interdiffusion grown organolead halide perovskite thin films by thermal annealing. *Journal of Materials Chemistry A*, *2*(43), 18508-18514.

Blazinic, V., Ericsson, L. K., Levine, I., Hansson, R., Opitz, A., & Moons, E. (2019). Impact of intentional photo-oxidation of a donor polymer and PC 70 BM on solar cell performance. *Physical Chemistry Chemical Physics*, *21*(40), 22259-22271.

Chen, Q., Wu, J., Ou, X., Huang, B., Almutlaq, J., Zhumekenov, A. A., ... & Liu, X. (2018). All-inorganic perovskite nanocrystal scintillators. *Nature*, *561*(7721), 88-93.

Coffey, A. H. (2023). *Quasi-Two-Dimensional Halide Perovskite Materials for Photovoltaic Applications* (Doctoral dissertation, Purdue University).

De Wolf, S., Holovsky, J., Moon, S. J., Loper, P., Niesen, B., Ledinsky, M., ...& Ballif, C. (2014). Organometallic halide perovskites: sharp optical absorption edge and its relation to photovoltaic performance. *The journal of physical chemistry letters*, *5*(6), 1035-1039.

Dittrich, T., Awino, C., Prajongtat, P., Rech, B., & Lux-Steiner, M. C. (2015). Temperature dependence of the band gap of CH3NH3PbI3 stabilized with PMMA: a modulated surface photovoltage study. *The Journal of Physical Chemistry C*, *119*(42), 23968-23972.

Doumbia, Y., Bouich, A., Soro, D., & Soucase, B. M. (2022). Mixed halide head perovskites thin films: Stability and growth investigation. *Optik*, *261*, 169222.

Dunlap-Shohl, W. A. (2019). *Novel Fabrication Approaches for Optoelectronic Halide Semiconductor Thin Films and Devices* (Doctoral dissertation, Duke University).

Fan, P., Gu, D., Liang, G. X., Luo, J. T., Chen, J. L., Zheng, Z. H., & Zhang, D. P. (2016). High-performance perovskite CH3NH3PbI3 thin films for solar cells prepared by single-source physical vapour deposition. *Scientific reports*, *6*(1), 29910.

Heo, J. H., Im, S. H., Noh, J. H., Mandal, T. N., Lim, C. S., Chang, J. A., ...& Seok, S. I. (2013). Efficient inorganic–organic hybrid heterojunction solar cells containing perovskite compound and polymeric hole conductors. *Nature photonics*, *7*(6), 486-491

Heo, J. H., Song, D. H., Han, H. J., Kim, S. Y., Kim, J. H., Kim, D., ... & Im, S. H. (2015). Planar CH3NH3PbI3 perovskite solar cells with constant 17.2% average power conversion efficiency irrespective of the scan rate. *Advanced Materials*, *27*(22), 3424-3430.

Huang, Y. T., Kavanagh, S. R., Scanlon, D. O., Walsh, A., & Hoye, R. L. (2021). Perovskite-inspired materials for photovoltaics and beyond—from design to devices. *Nanotechnology*, *32*(13), 132004.

Jeon, N. J., Noh, J. H., Kim, Y. C., Yang, W. S., Ryu, S., & Seok, S. I. (2014). Solvent engineering for high-performance inorganic–organic hybrid perovskite solar cells. *Nature materials*, *13*(9), 897-903.

Jiang, J., Vicent-Luna, J. M., & Tao, S. (2022). The role of solvents in the formation of methylammonium lead triiodide perovskite. *Journal of Energy Chemistry*, *68*, 393-400.

Kegelmann, L., Wolff, C. M., Awino, C., Lang, F., Unger, E. L., Korte, L., ... & Albrecht, S. (2017). It Takes Two to Tango□ Double-Layer Selective Contacts in Perovskite Solar Cells for Improved Device Performance and Reduced Hysteresis. *ACS applied materials & interfaces*, *9*(20), 17245-17255

Konstantakou, M., Perganti, D., Falaras, P., & Stergiopoulos, T. (2017). Anti-solvent crystallization strategies for highly efficient perovskite solar cells. *Crystals*, *7*(10), 291.

Lee, J. W., Kim, H. S., & Park, N. G. (2016). Lewis acid–base adduct approach for high efficiency perovskite solar cells. *Accounts of chemical research*, *49*(2), 311-319.

Li, D., Bretschneider, S. A., Bergmann, V. W., Hermes, I. M., Mars, J., Klasen, A., ... & Berger, R. (2016). Humidity-induced grain boundaries in MAPbI3 perovskite films. *The Journal of Physical Chemistry C*, *120*(12), 6363-6368.

Liu, J., Wang, G., Luo, K., He, X., Ye, Q., Liao, C., & Mei, J. (2017). Understanding the role of the electron-transport layer in highly efficient planar perovskite solar cells. *ChemPhysChem*, *18*(6), 617-625.

Liu, R., & Xu, K. (2020). Solvent engineering for perovskite solar cells: a review. *Micro & Nano Letters*, *15*(6), 349-353.

Marciniak, S., Crispin, X., Uvdal, K., Trzcinski, M., Birgerson, J., Groenendaal, L., ...& Salaneck, W. R. (2004). Light induced damage in poly (3, 4-ethylenedioxythiophene) and its derivatives studied by photoelectron spectroscopy. *Synthetic metals*, *141*(1-2), 67-73.

Omondi, C. A. (2018). *Investigation of hybrid organic-inorganic lead halide perovskites by modulated surface photovoltage spectroscopy*. Technische Universitaet Berlin (Germany).

Prajongtat, P., & Dittrich, T. (2015). Precipitation of CH3NH3PbCl3 in CH3NH3PbI3 and its impact on modulated charge separation. *The Journal of Physical Chemistry C*, *119*(18), 9926-9933.

Rong, Y., Tang, Z., Zhao, Y., Zhong, X., Venkatesan, S., Graham, H., ...& Yao, Y. (2015). Solvent engineering towards controlled grain growth in perovskite planar heterojunction solar cells. *Nanoscale*, *7*(24), 10595-10599.

Shockley, W., & Queisser, H. (2018). Detailed balance limit of efficiency of p–n junction solar cells. In *Renewable energy* (pp. Vol2_35-Vol2_54). Routledge.

Singh, M., Abdelsamie, M., Li, Q., Kodalle, T., Lee, D. K., Arnold, S., ... & Sutter-Fella, C. M. (2023). Effect of the precursor chemistry on the crystallization of triple cation mixed halide perovskites. *Chemistry of Materials*, *35*(18), 7450-7459.

Stranks, S. D. (2017). Nonradiative losses in metal halide perovskites. *ACS Energy Letters*, *2*(7), 1515-1525.

Taylor, A. D., Sun, Q., Goetz, K. P., An, Q., Schramm, T., Hofstetter, Y., ... & Vaynzof, Y. (2021). A general approach to high-efficiency perovskite solar cells by any antisolvent. *Nature communications*, *12*(1), 1878.

Toloueinia, P., Khassaf, H., Shirazi Amin, A., Tobin, Z. M., Alpay, S. P., & Suib, S. L. (2020). Moisture-induced structural degradation in methylammonium lead iodide perovskite thin films. *ACS Applied Energy Materials*, *3*(9), 8240-8248.

Wang, F., Han, Y., Duan, D., Ge, C., Hu, H., & Li, G. (2022). Recent progress of scalable perovskite solar cells and modules. *Energy Reviews*, *1*(2), 100010.

Wu, T., Qin, Z., Wang, Y., Wu, Y., Chen, W., Zhang, S., ... & Han, L. (2021). The main progress of perovskite solar cells in 2020–2021. *Nano-Micro Letters*, *13*, 1-18.

Xu, J., Dai, J., Dong, H., Li, P., Chen, J., Zhu, X., ...& Wu, Z. (2022). Surface-tension release in PTAA-based inverted perovskite solar cells. *Organic Electronics*, *100*, 106378.

Zhang, N., Zhang, Z., Liu, T., He, T., Liu, P., Li, J., ... & Yuan, M. (2023). Efficient and stable MAPbI3 perovskite solar cells via green anti-solvent diethyl carbonate. *Organic Electronics*, *113*, 106709.